

# Magnetism at the interface between ferromagnetic and superconducting oxides

J. CHAKHALIAN<sup>1,2\*</sup>, J. W. FREELAND<sup>3</sup>, G. SRAJER<sup>3</sup>, J. STREMPFER<sup>1</sup>, G. KHALIULLIN<sup>1</sup>, J. C. CEZAR<sup>4</sup>, T. CHARLTON<sup>5</sup>, R. DALGLIESH<sup>5</sup>, C. BERNHARD<sup>1</sup>, G. CRISTIANI<sup>1</sup>, H.-U. HABERMEIER<sup>1</sup> AND B. KEIMER<sup>1</sup>

<sup>1</sup>Max Planck Institute for Solid State Research, Stuttgart D-70561, Germany

<sup>2</sup>University of Arkansas, Fayetteville, Arkansas 72701, USA

<sup>3</sup>Argonne National Laboratory, Argonne, Illinois 60439, USA

<sup>4</sup>European Synchrotron Radiation Facility, 38043 Grenoble, CEDEX 9, France

<sup>5</sup>ISIS Facility, Rutherford Appleton Laboratory, Chilton, Didcot, Oxon OX11 0QX, UK

\*e-mail: j.chakhalian@fkf.mpg.de

Published online: 1 April 2006; doi:10.1038/nphys272

**C**arefully controlled interfaces between two materials can give rise to novel physical phenomena and functionalities not exhibited by either of the constituent materials alone. Modern synthesis methods have yielded high-quality heterostructures of oxide materials with competing order parameters. Although magnetic correlations at the interface are expected to be important in determining the macroscopic properties of such systems, a quantitative determination of the interfacial magnetization profile has thus far not been reported. Here we examine superlattices composed of the half-metallic ferromagnet  $\text{La}_{2/3}\text{Ca}_{1/3}\text{MnO}_3$  and the high-temperature superconductor  $\text{YBa}_2\text{Cu}_3\text{O}_7$  by absorption spectroscopy with circularly polarized X-rays and by off-specular neutron reflectometry. The resulting data yield microscopic insight into the interplay of spin and orbital degrees of freedom at the interface. The experiments also reveal an extensive rearrangement of the magnetic domain structure at the superconducting transition temperature. This methodology establishes an incisive probe of the interplay between competing electronic order parameters in oxide heterostructures.

Electronic interface phenomena in simple metals and semiconductors have been extensively investigated during the past three decades. Prominent examples include the quantum Hall effect in semiconductor heterostructures, and the ‘giant magnetoresistance’ effect in superlattices of elemental metals. Modern synthesis methods have also allowed detailed experiments on heterostructures whose constituents have mutually incompatible order parameters. In particular, experiments on trilayer sandwiches comprising elemental singlet superconductors and ferromagnets have revealed a sign alternation of the superconducting phase in adjacent layers, as well as hints of an oscillatory dependence of the superconducting transition temperature on the ferromagnetic layer thickness, as predicted by theory<sup>1,2</sup>.

Recently, the synthesis of transition metal oxide heterostructures with atomic-scale precision has opened

new perspectives for the investigation of electronic interface phenomena. The unusual quantum states realized in bulk transition metal oxides have been at the forefront of solid-state physics for the past two decades<sup>3,4</sup>. Among these, high-temperature superconductivity in copper oxides and fully spin-polarized (‘half-metallic’) ferromagnetism in manganese oxides have received particular attention. High-quality cuprate-manganite superlattices have recently been prepared, and initial work has already revealed intriguing macroscopic phenomena, such as giant magnetoresistance and proximity-induced metal–insulator transitions<sup>5–7</sup>. However, the microscopic mechanisms underlying these phenomena are almost entirely unexplored. Heuristically, as the valence electrons in both cuprates and manganites are subject to strong magnetic interactions, the magnetization at the interface is expected to have a profound influence on the charge transport in these systems. However, very little is known about the interfacial magnetization profile. Here we show that the combination of two experimental methods, X-ray magnetic circular dichroism (XMCD) and neutron reflectometry, yields a detailed microscopic picture of the magnetization profile both parallel and perpendicular to the superlattice plane, and offers intriguing insight into the interplay between ferromagnetism and superconductivity at the interface.

XMCD is the difference between absorption spectra for left- and right-polarized X-rays. The measurement involves changing the magnetization direction at each energy point of the absorption curve to measure the absorption, with photon helicity and magnetization parallel ( $I^+$ ) and antiparallel ( $I^-$ ). The sum ( $I^+ + I^-$ ) provides electronic information, whereas the XMCD ( $I^+ - I^-$ ) is magnetic in origin and yields the element-specific net magnetization. Owing to its monolayer sensitivity and a typical penetration depth of several hundred ångströms, XMCD is well suited to investigations of nanoscale magnetism at ‘buried’ interfaces<sup>8</sup>. A sketch of the experimental setup is shown in Fig. 1a.

Figure 2a shows representative Cu and Mn XMCD spectra on a superlattice of alternating 100-Å-thick, *c*-axis-oriented  $\text{YBa}_2\text{Cu}_3\text{O}_7$

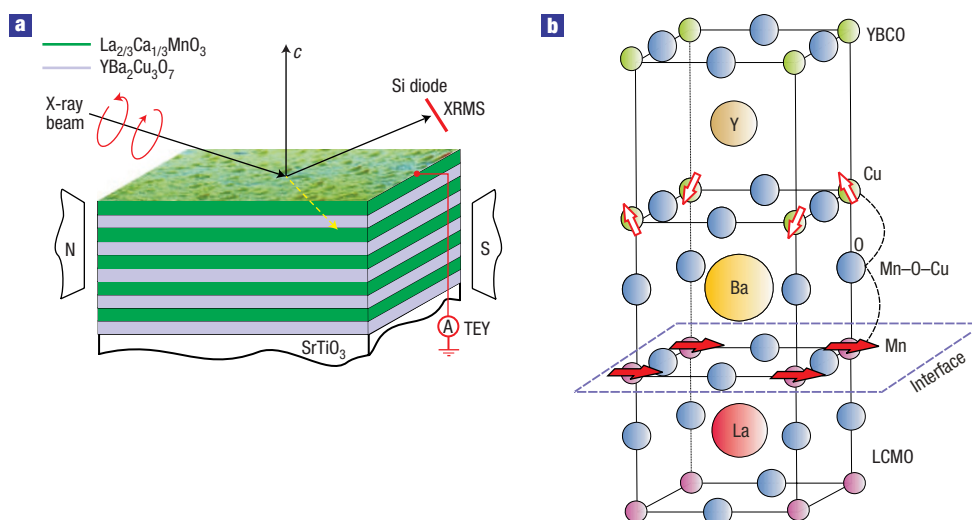


**Figure 1** XMCD and XRMS experimental setup and atomic stacking structure at the interface. **a**, Schematic diagram of the experimental setup used to obtain the XMCD and XRMS data. To obtain a sizable magnetic dichroism, the film plane is tilted with respect to the photon beam propagation direction. The overall structural roughness for the superlattices is  $\sim 5 \text{ \AA}$  (ref. 14). **b**, Atomic stacking sequence and arrangement of atoms at the YBCO/LCMO interface. The YBCO layer growth starts from a sub-unit cell with no Cu chains<sup>16</sup>. The solid red arrows show the Mn magnetic moments, whereas the white arrows mark a possible arrangement of the induced magnetic moments on Cu. The relative orientation of the net magnetic moments is derived from the sign of the magnetic dichroism at the Cu and Mn  $L_3$  edges.

(YBCO) and  $\text{La}_{2/3}\text{Ca}_{1/3}\text{MnO}_3$  (LCMO) layers taken at the resonant  $L_{2,3}$  edges ( $2p \rightarrow 3d$  transition) at 30 K. Magnetic dichroism is clearly present at both Mn and Cu edges. As the manganite layers undergo a ferromagnetic transition at around 180 K, the large dichroism at the Mn edge is expected. However, the presence of a net ferromagnetic magnetization on Cu is surprising. We ruled out experimental artefacts by confirming that measurements of XMCD in two different modes (changing photon helicity for a fixed field, and changing magnetization direction for fixed helicity) resulted in the same answer. Thus, the data provide clear evidence for the presence of an uncompensated induced magnetic moment in the YBCO layer close to the LCMO interface. As seen in Fig. 2a, the Cu dichroism is small compared with that of Mn ( $\sim 27\%$ ), and does not exceed 1.4%. The mutual orientation of the Mn and Cu magnetic moments can be deduced from the relative sign of the  $L_3$  peaks for the same helicity of light. Figure 2a demonstrates that the Mn and Cu  $L_3$  peaks have opposite signs, which indicates an antiparallel orientation of the corresponding magnetic moments.

To investigate the origin of the ferromagnetic polarization of Cu, we carried out XMCD measurements over a wide range of temperatures at both Mn and Cu edges. Figure 2b shows the resulting data compared with the bulk magnetization of the entire sample as determined by superconducting quantum interference device (SQUID) magnetometry. At temperatures above 170 K, the dichroism on Mn disappears, consistent with the ferromagnet-paramagnet transition at  $T_M$ . The temperature dependence of the XMCD signal deviates from that of the bulk magnetization, especially in the surface-sensitive total electron yield (TEY) mode. The reduced magnetization at the topmost interface is consistent with previous measurements on thin films and superlattices, and is believed to result from the lower atomic coordination at the interface<sup>9–11</sup>. An analogous behaviour was also found for Cu, except that above 150 K its XMCD signal decreases below the detection limit. The rescaled dichroic signal of Cu closely follows that of Mn. The similar temperature dependence of both signals indicates that the magnetic moment on Cu is induced by strong interactions

between Cu spins and the ferromagnetic moment of Mn across the interface.

To determine quantitatively the interfacial magnetization profile, we used the XMCD sum rules<sup>12,13</sup> to separate the orbital ( $\mu_l$ ) and spin ( $\mu_s$ ) contributions to the total ferromagnetic moment. Assuming that the main intensity in the X-ray absorption originates from a single hole in the  $3d^9$  state, we set an upper limit of  $\mu_l \leq 0.01 \mu_B/\text{Cu}$  averaged over the entire sample;  $\mu_B$  is the Bohr magnetron. This small value is expected because the orbital moment in YBCO is quenched. The averaged spin part of the magnetization is estimated as  $0.06 \mu_B/\text{Cu}$  at 10 K. Comparison to previous specular neutron reflectivity results on the same samples<sup>14</sup> allows us to reconstruct the full magnetization profile. Because of the lack of phase information inherent in neutron reflectivity measurements, the neutron data were compatible with two physically very different scenarios: (1) a 20-Å-thick magnetically disordered ('dead') layer in LCMO and completely non-magnetic cuprate layers; and (2) a 10-Å-thick layer with a suppressed (but non-zero) ferromagnetic moment in LCMO antiferromagnetically coupled to an approximately 20-Å-thick spin-polarized layer in YBCO. The XMCD measurements reported here uniquely select scenario (2). This demonstrates that the Cu polarization is confined to the proximity of the interface. Assuming an exponential decay of the ferromagnetic Cu spin moment away from the interface, its amplitude is estimated as  $\mu_s \sim 0.2 \mu_B/\text{Cu}$  in the  $\text{CuO}_2$  layer directly adjacent to LCMO.

The atomic arrangement at the interface known from previous electron-diffraction work<sup>15,16</sup> (Fig. 1b) shows that the antiferromagnetic interaction  $J'$  across the interface competes with the antiferromagnetic superexchange coupling between nearest-neighbour Cu spins within a copper oxide layer. As the latter interaction is large ( $J \sim 100 \text{ meV}$ ), the measured ferromagnetic polarization of Cu is probably due to spin canting. To estimate the magnitude of  $J'$ , we assume that the first copper oxide layer is depleted of holes, such that each Cu atom carries a localized magnetic moment  $\mu \sim 1\mu_B$ . This approximation is not unrealistic, because the  $\text{CuO}$  chains, which act as the hole reservoir

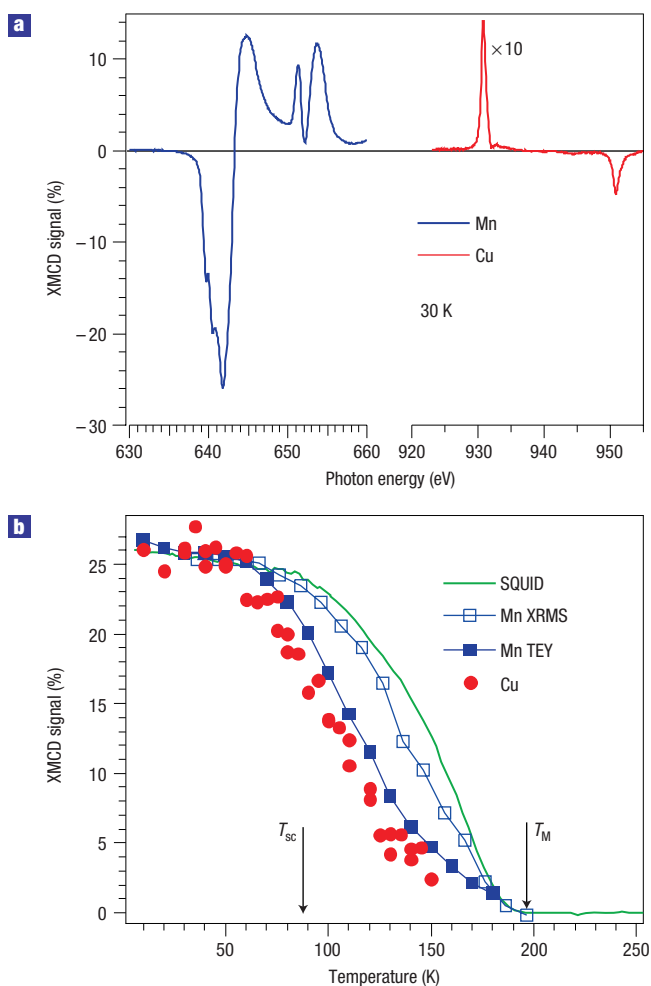


**Figure 2** XMCD spectra and their evolution with temperature. **a**, XMCD signals obtained from the core-level absorption spectra for Cu and Mn. The Mn XMCD signal (blue curve) is large and reaches 23% at the  $L_3$  edge. For comparison, the magnitude of the XMCD signal of Cu (red curve) is multiplied by a factor of 10. **b**, Temperature dependence of the XMCD signals of Cu and Mn compared with the bulk magnetization (green line). All curves are normalized to the value of dichroism on Mn. The interfacial magnetism of Mn decreases faster than the bulk magnetization. The estimated errors are of the order of 20% at low temperatures, and become larger as the temperature approaches  $T_M$ .

of YBCO, are missing in the unit cell directly adjacent to the interface (Fig. 1b), and it is consistent with the observation of a rapidly decreasing superconducting transition temperature,  $T_{SC}$ , with decreasing YBCO layer thickness<sup>17</sup>. A simple calculation with this assumption shows that  $J'/J \sim 2\mu_s/\mu \sim 0.4$ . The large magnitude of  $J'$  explains the parallel temperature evolution of Cu and Mn ordered moments shown in Fig. 2b.

Initially, the antiferromagnetic sign of the coupling across the interface appears to be inconsistent with the Goodenough–Kanamori–Anderson rules for exchange interactions in oxides. Figure 1b shows that this coupling is mediated by a  $180^\circ$  Mn–O–Cu exchange path bridging the interface. Although the conduction electrons in bulk YBCO reside in the  $d_{x^2-y^2}$  orbital, the ground state of bulk ferromagnetic metallic LCMO is believed to be an orbitally disordered state with fluctuating occupancy of  $d_{x^2-y^2}$  and  $d_{3z^2-r^2}$  orbitals<sup>18</sup>. If this electronic structure were maintained at the interface, the dominant contribution to the

Mn–O–Cu superexchange interaction would be provided by Cu  $d_{3z^2-r^2}$  electrons hopping into the partially occupied Mn<sup>3+</sup>  $d_{3z^2-r^2}$  orbital. The intra-atomic Hund's rule interaction on a Cu site in the intermediate state then results in a ferromagnetic superexchange interaction.

Therefore, the antiferromagnetic coupling observed implies that the orbital occupation on one or both sides of the interface is different from the bulk. On the YBCO side, occupation of the  $d_{x^2-y^2}$  orbital is expected to be maintained because of the robust crystal field and strong covalent bonding in the copper oxide layers. Supplementary linear polarization-dependent X-ray absorption spectroscopy measurements directly confirm this expectation (see the Supplementary Information). In contrast, on the LCMO side, the planar electrostatic environment of Mn ions at the interface is quite different from that in the three-dimensional bulk lattice structure. This situation can easily lead to a polarization of the orbital 'liquid'. In analogy to layered manganites<sup>19</sup>, it is expected that the  $d_{x^2-y^2}$  orbital will be preferentially occupied. The dominant superexchange interaction in this case is mediated by Cu  $d_{3z^2-r^2}$  electrons hopping into the empty Mn<sup>3+</sup>  $d_{3z^2-r^2}$  orbital. The Hund's rule interaction in the intermediate state then leads to an antiferromagnetic coupling, as observed. The magnitude of the superexchange coupling in this scenario can be estimated as  $J'/J \sim (4/9)(2J_H^{Mn}/E_{CuMn})(2J_H^{Cu}/E_{CuMn})$ , where  $E_{CuMn}$  is the energy associated with the charge transfer between a Cu ion and its nearest-neighbour Mn ion across the interface, and  $J_H$  is the Hund's rule coupling. With  $J_H = 1.19$  and  $0.89$  eV for Cu and Mn ions, respectively<sup>20</sup>, and  $E_{MnCu} \sim 2-3$  eV, we obtain  $J'/J \sim 0.2-0.4$ , consistent with the experimental situation presented above. In addition to the virtual hopping described above, there is another contribution associated with hopping of  $d_{3z^2-r^2}$  electrons of Cu to Mn<sup>4+</sup> sites that are also present in the LCMO layer. This process is similar to a double exchange, but it is also antiferromagnetic as the  $d_{3z^2-r^2}$  orbital of Cu is full, and the same orbital on the Mn<sup>4+</sup> site is completely empty. With the single, plausible assumption of a dominant occupation of the Mn  $d_{x^2-y^2}$  orbital at the interface, we thus obtain a quantitatively consistent description of interfacial magnetism in the superlattice.

Having obtained a detailed picture of the magnetization profile perpendicular to the superlattice plane, we now turn to the lateral magnetization. To this end, we carried out off-specular neutron-scattering experiments in the presence of an in-plane magnetic field below the field required to saturate the magnetic hysteresis loop. Representative data displayed in Fig. 3 illustrate the thermal evolution of the neutron reflectivity as a function of the in-plane and out-of-plane wavevectors,  $Q_x$  and  $Q_z$ .

In the following, we focus on the first Bragg peak around  $Q_z = 0.03 \text{ \AA}^{-1}$ , whose intensity consists of both structural and magnetic contributions. As the temperature is lowered below the magnetic transition at  $T_M = 180$  K, the Bragg peak intensity increases as expected (see Fig. 3a). The absence of any significant diffuse intensity around the Bragg peak is evidence of the small magnitude of the in-plane magnetic roughness throughout the multilayer. As the temperature is lowered below 105 K, the Bragg peak broadens slightly in the off-specular direction (Fig. 3b). Comparison with previous microscopy work on LCMO films on SrTiO<sub>3</sub> (STO) substrates<sup>21</sup> shows that this effect probably originates from the cubic-to-tetragonal phase transition of the STO substrate at  $T_S = 105$  K, which is associated with crystallographic twin formation and buckling of the substrate surface. The neutron data of Fig. 3 demonstrate that the substrate-induced modulation permeates the entire superlattice.

A few degrees below  $T_{SC}$ , a new dramatic change in the in-plane diffraction pattern around the Bragg reflection is observed. As seen in the representative data of Fig. 3c, the off-specular

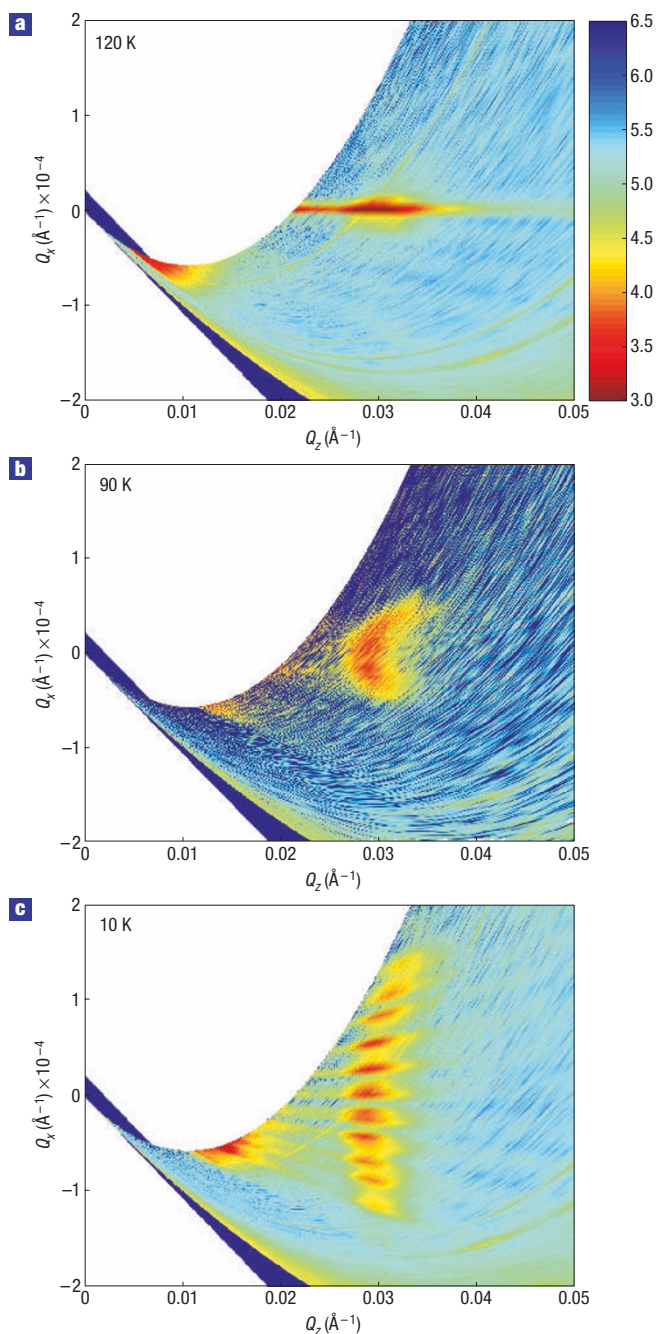


**Figure 3** Off-specular neutron reflectivity taken at several characteristic temperatures. Thermal evolution of the specular and off-specular neutron intensity represented by  $Q_x$ - $Q_z$  maps around the first superlattice Bragg reflection. Representative data are shown in three characteristic temperature regimes: **a**,  $T = 120$  K, below the onset of ferromagnetism at  $T_M = 180$  K; **b**,  $T = 90$  K, below the structural transition in the STO substrate at 105 K; and **c**,  $T = 10$  K, below the superconducting transition temperature  $T_{SC} = 78$  K.

intensity abruptly expands into a much wider band, whereas the peak intensity is approximately conserved. The diffraction pattern below  $T_{SC}$  consists of a series of sharp peaks as a function of  $Q_x$ . This is characteristic of a stripe-like magnetic domain pattern in real space. Both the separation between the peaks (inversely proportional to the size of the magnetic domains,  $d$ ) and the overall width of the pattern (inversely related to the width of the

domain walls,  $\delta$ ) are strongly temperature dependent. For instance, at  $T = 63$  and 10 K the parameters extracted from the data are  $d \approx 41 \mu\text{m}$  and  $\delta \approx 3 \mu\text{m}$ , and  $d \approx 24 \mu\text{m}$  and  $\delta \approx 2 \mu\text{m}$ , respectively. We interpret the appearance of this pattern below  $T_{SC}$  as follows. The large length scale of the observed modulation indicates that electrodynamic (rather than exchange) forces are responsible for the interaction between superconductivity and ferromagnetism. As the  $c$ -axis Josephson penetration depth of YBCO is much larger than the thickness of the YBCO layers, the superlattice is essentially transparent to the in-plane magnetic field applied in the neutron experiment. However, if Abrikosov vortices are nucleated below  $T_{SC}$ , possibly by the substrate-induced structural modulation discussed above, electrodynamic interactions between these vortices and the ferromagnetic manganite layers could lead to the unusual domain state that we observed.

## METHODS

The superlattices were grown on a 0.5-mm-thick, atomically flat STO (001) substrate by pulsed laser deposition (Fig. 1a). A KrF excimer laser ( $\lambda = 248$  nm) with a repetition rate of 2 Hz was used to ablate the sintered stoichiometric targets, with a laser energy density of  $\sim 2 \text{ J cm}^{-2}$  at the target position. The superlattices were grown at a temperature of 730 °C, under an oxygen partial pressure of 0.5 mbar. After growth, the samples were annealed *in situ* for 1 h at 530 °C in 1,000 mbar of pure oxygen.

It is well known that epitaxial strain profoundly affects the magnetic properties of thin manganite films grown on STO<sup>22–24</sup>. On the other hand, YBCO and LCMO are nearly perfectly lattice matched. By using YBCO as a ‘buffer’ layer directly deposited on the STO substrate, the effect of strain was essentially removed<sup>25</sup>. Because of the sensitivity of thin YBCO layers to moisture, the superlattices were terminated with a LCMO layer, which is much more stable against surface degradation. An extensive set of characterization measurements (see the Supplementary Information) confirmed the atomic-scale perfection of the interfaces of our superlattices. Bulk transport and magnetic measurements (see the Supplementary Information) demonstrate an onset of ferromagnetism at  $T_M \sim 180$  K, and a superconducting transition at  $T_{SC} \sim 78$  K. Both transition temperatures are lower than those observed in the constituent bulk materials, possibly due to interactions between the competing order parameters. The strong suppression of the resistivity with applied magnetic field (see Supplementary Information, Fig. S1B) reflects the well known ‘colossal magnetoresistance’ effect in the manganite layers.

The XMCD experiments were carried out at beamline 4-ID-C at the Advanced Photon Source, and ID08 of the European Synchrotron Radiation Facility. We used circularly polarized soft X-rays at the L-absorption edges of Mn and Cu. During the experiments, TEY, X-ray magnetic reflectivity (XRMS), and fluorescence yield data were recorded simultaneously. The surface-sensitive TEY mode was used to acquire information about magnetism at the top-most interface, whereas the XRMS and fluorescence yield modes allowed us to probe deeper layers. All of the XMCD spectra were measured in remanence, and in an applied field of 500 Oe. The off-specular neutron reflectivity data were obtained at the CRISP (ISIS, Rutherford Appleton Laboratory) operating at grazing incidence in a time-of-flight mode with a bandpass of  $0.5 \text{ \AA} < \lambda < 6.5 \text{ \AA}$ . The  $Q$ -space maps were recorded with a 256-channel multidetector. During the measurements an external magnetic field of 1,000 Oe was applied in the plane of the superlattice.

Received 5 January 2006; accepted 28 February 2006; published 1 April 2006.

## References

- Buzdin, A. Proximity effects in superconductor-ferromagnet heterostructures. *Rev. Mod. Phys.* **77**, 935–976 (2005).
- Lyuksyutov, I. F. & Pokrovsky, V. L. Ferromagnet-superconductor hybrids. *Adv. Phys.* **54**, 67–136 (2005).
- Dagotto, E. Complexity in strongly correlated electronic systems. *Science* **309**, 257–262 (2005).
- Tokura, Y. & Nagaosa, N. Orbital physics in transition-metal oxides. *Science* **288**, 462–468 (2000).
- Sefrioui, Z. *et al.* Ferromagnetic/superconducting proximity effect in  $\text{La}_{0.7}\text{Ca}_{0.3}\text{MnO}_3/\text{YBa}_2\text{Cu}_3\text{O}_{7-s}$  superlattices. *Phys. Rev. B* **67**, 214511–214515 (2003).
- Przyłuski, P. *et al.* Magnetic properties of  $\text{La}_{0.67}\text{Sr}_{0.33}\text{MnO}_3/\text{YBa}_2\text{Cu}_3\text{O}_7$  superlattices. *Phys. Rev. B* **69**, 134428–134435 (2004).
- Peña, V. *et al.* Giant magnetoresistance in ferromagnet/superconductor superlattices. *Phys. Rev. Lett.* **94**, 057002–057006 (2005).
- Stöhr, J. Exploring the microscopic origin of magnetic anisotropies with X-ray magnetic circular dichroism (XMCD) spectroscopy. *J. Magn. Mater.* **200**, 470–497 (1999).
- Yamada, H. *et al.* Engineered interface of magnetic oxides. *Science* **305**, 646–648 (2004).

- Park, J.-H. *et al.* Magnetic properties at surface boundary of a half-metallic ferromagnet  $\text{La}_{0.7}\text{Sr}_{0.3}\text{MnO}_3$ . *Phys. Rev. Lett.* **81**, 1953–1956 (1998).
- Kanki, T. *et al.* Anomalous strain effect in  $\text{La}_{0.8}\text{Ba}_{0.2}\text{MnO}_3$  epitaxial thin film: Role of the orbital degree of freedom in stabilizing ferromagnetism. *Phys. Rev. B* **64**, 224418–224423 (2001).
- Chen, C. T. *et al.* Experimental confirmation of the X-ray magnetic circular dichroism sum rules for iron and cobalt. *Phys. Rev. Lett.* **75**, 152–155 (1995).
- Thole, B. T., Carra, P., Sette, F. & van der Laan, G. X-ray circular dichroism as a probe of orbital magnetization. *Phys. Rev. Lett.* **68**, 1943–1946 (1992).
- Stahn, J. *et al.* Magnetic proximity effect in perovskite superconductor/ferromagnet multilayers. *Phys. Rev. B* **71**, 140509–140513 (2005).
- Matijasevic, V. C. *et al.* Nucleation of a complex oxide during epitaxial film growth:  $\text{SmBa}_2\text{Cu}_3\text{O}_7$  on  $\text{SrTiO}_3$ . *Phys. Rev. Lett.* **76**, 4765–4768 (1996).
- Varela, M. *et al.* Nanoscale analysis of  $\text{YBa}_2\text{Cu}_3\text{O}_{7-x}/\text{La}_{0.67}\text{Ca}_{0.33}\text{MnO}_3$  interfaces. *Solid-State Electron.* **47**, 2245–2248 (2003).
- Holden, T. *et al.* Proximity induced metal-insulator transition in  $\text{YBa}_2\text{Cu}_3\text{O}_7/\text{La}_{2/3}\text{Ca}_{1/3}\text{MnO}_3$  superlattices. *Phys. Rev. B* **69**, 64505–64512 (2004).
- Imada, M., Fujimori, A. & Tokura, Y. Metal-insulator transitions. *Rev. Mod. Phys.* **70**, 1039–1263 (1998).
- Kimura, T. & Tokura, Y. Layered magnetic manganites. *Annu. Rev. Mater. Sci.* **30**, 451–474 (2000).
- Griffith, J. S. *The Theory of Transition-Metal Ions* (Cambridge Univ. Press, Cambridge, 1961).
- Vlasko-Vlasov, V. K. *et al.* Direct magneto-optical observation of a structural phase transition in thin films of manganites. *Phys. Rev. Lett.* **84**, 2239–2242 (2000).
- Razavi, F. *et al.* Epitaxial strain induced metal insulator transition in  $\text{La}_{0.9}\text{Sr}_{0.1}\text{MnO}_3$  and  $\text{La}_{0.88}\text{Sr}_{0.12}\text{MnO}_3$  thin films. *Appl. Phys. Lett.* **76**, 155–157 (2000).
- Prellier, W., Rajeswari, M., Venkatesan, T. & Greene, R. L. Effects of annealing and strain on  $\text{La}_{1-x}\text{Ca}_x\text{MnO}_3$  thin films: A phase diagram in the ferromagnetic region. *Appl. Phys. Lett.* **75**, 1446–1448 (1999).
- Praus, R. B. *et al.* Effects of strain on the properties of  $\text{La}_{0.67}\text{Ca}_{0.33}\text{MnO}_3$  thin films. *J. Magn. Magn. Mater.* **211**, 41–46 (2000).
- Yang, Z. Q. *et al.* Strain release of  $(\text{La},\text{Ca})\text{MnO}_3$  thin films by  $\text{YBa}_2\text{Cu}_3\text{O}_{7-x}$ . *Phys. Rev. B* **67**, 024408–0244013 (2003).

#### Acknowledgements

The authors would like to acknowledge S. Okamoto, A. Millis and R. K. Kremer for useful discussions and skilled experimental assistance. Work at Argonne National Laboratory is supported by the United States Department of Energy, Office of Basic Energy Sciences, under contract No. W-31-109-ENG-38. Correspondence and requests for materials should be addressed to J.C. Supplementary Information accompanies this paper on [www.nature.com/naturephysics](http://www.nature.com/naturephysics).

#### Competing financial interests

The authors declare that they have no competing financial interests.

Reprints and permission information is available online at <http://npg.nature.com/reprintsandpermissions/>